

Fermion Loops, Linear Magnetoresistance, Linear In Temperature Resistance, and Superconductivity

Vincent Sacksteder*

Department of Physics, Royal Holloway University of London, United Kingdom

We show that if one performs a Fourier transform with respect to magnetic field of a sample's magnetoconductance, one obtains a curve describing the areas of the loops traced by electrons and holes within the sample. Linear magnetoresistance is a signal that the electron loops are larger and obey a different scaling law than in ordinary materials, and the linear in temperature resistance seen in cuprates and pnictides is the $B = 0$ manifestation of linear magnetoresistance. Both effects are a manifestation of quantum interference similar to weak antilocalization, but with an extra level of quantum coherence. We find excellent agreement with experimental measurements of the linear coefficients of these effects in the cuprates and pnictides. Lastly we analyze T_c and the pseudogap temperature T_{pg} in terms of temperature-limited quantum coherence and discuss prospects for increasing T_c .

In atomic units $m_e = e = \hbar = k_B = 1$ the magnetic field B has dimensions of inverse area, which is key to understanding the electrical conductance's dependence on B . Large fields probe areas at the scale of the unit cell, and small changes in field probe much larger areas. At large fields one finds Landau levels and Schubnikov-de Haas (SdH) oscillations, which are visible in the longitudinal conductance $G_{xx}(B)$ as peaks at characteristic field strengths determined by the Fermi energy E_F . The Fermi surface's cross section, an inverse area, can be read off from the peak positions. At small fields one finds weak (anti) localization (WL/WAL), where quantum interference causes G_{xx} to decrease or increase with field depending on whether the spin relaxation length l_s is small or large.

Recent years have exposed mysteries which lie well beyond traditional SdH and WL physics. Many experiments report systems where the longitudinal resistance R_{xx} increases linearly with B and does not saturate.^{1–11} This contrasts both with SdH oscillations which are periodic in $1/B$ and with WL which is logarithmic. Explanations have been given for the cases of ballistic conduction when the Fermi surface has a cusp, of a 3-D Dirac cone in the presence of a strong magnetic field, of a density gradient across the sample, and of classical transport with strong sample inhomogeneities.^{12–16} However this kind of case by case treatment is not entirely satisfactory given the wide range of experimental realizations.

Another long-standing mystery is that in cuprates and pnictides outside of the superconducting phase the resistance increases linearly with temperature and does not saturate.¹⁷ This is inconsistent both with the WAL signal which increases much more slowly with T (logarithmically in 2-D and as a square root in 3-D) and with phonon based scattering which should saturate at a maximum determined by the atomic spacing. Materials whose resistance is linear in temperature are called bad metals and are understood to be strongly correlated, but the details of the conduction process responsible for linear resistance are not understood. Very recently the linear dependence on temperature has been linked to linear magnetoresis-

tance found in the same bad metal regime.^{18,19}

This paper, inspired by the magnetic field's units, develops a geometric analysis of magnetotransport in terms of loops, fluxes through those loops, and the Aharonov-Bohm effect. We show that this interpretation is very powerful - it is rooted in charge conservation, allows no renormalization of its constants by any physical process, and gives immediate insight into magnetotransport at both strong and weak fields.

We use the geometrical analysis to argue that linear magnetoresistance is a manifestation of weak antilocalization, with the addition of certain interference effects which lead to a linear instead of logarithmic signal. The resistance's increase rather than decrease with field indicates that the spin relaxation length l_s is short, which is the case if there are large magnetic fluctuations, if the spin-orbit interaction is strong, or if spin is strongly correlated. The bad metals' linear-in-temperature resistance, in our view, is nothing other than the zero-field manifestation of the linear magnetoresistance.

Our explanation of the linear-in-temperature resistance contrasts with most other work on bad metals, which typically neglects WAL and therefore deduces that the scattering time scale is the inverse of temperature, opening up a range of questions about correlation effects at short time scales.¹⁷ We claim instead that the resistance is controlled by quantum scattering processes with an extra level of coherence. We do however have two things in common with other theories of bad metals: we locate the source of the quantum coherence in electronic correlations, and we find that the electrons in play have a characteristic energy scale which is independent of the underlying band structure.^{20,21}

We found our geometric analysis of magnetotransport on a basic result from relativistic quantum field theory: the unique way to build a theory of fermions which conserves charge is to first add a phase degree of freedom $\phi(\vec{x})$ (a $U(1)$ phase for electromagnetism) and then require that the theory be invariant under multiplications by $\exp(i\phi)$. After rigorous development one obtains two requirements which constrain every condensed matter

theory:

- The effect of an external magnetic field \vec{B} on electrons must be mediated by the minimal coupling: the momentum operator \vec{p} must be replaced by $\vec{p} - e\vec{R}$, where \vec{R} is the gauge field determining the magnetic field by $\vec{B} = \vec{\nabla} \times \vec{R}$.
- All physical observables must be invariant under gauge transformations of $\vec{R} \rightarrow \vec{R} + \vec{\nabla}\phi$, no matter what value of $\phi(\vec{x})$ is chosen.

These requirements have very important consequences for the structure of any physical observable. The only way to build a gauge invariant observable \mathcal{O} from the minimal coupling is by requiring each electron or hole contributing to the observable to return to its starting position, forming closed loops. The actual shape and size of the loops, and also the number of loops, is completely unrestricted by gauge invariance; the emphasis is on their closed nature. It is important to be clear that the loops under discussion here are traced by bare electrons and holes, which may have very little to do with whether a system is a Fermi liquid, or whether it has any quasiparticles at all.

Because each electron is required to trace a loop, the only way that a magnetic field can affect any observable is by introducing a multiplicative factor, the Wilson loop $W_\Gamma = \exp(i \oint_\Gamma d\vec{x} \cdot \vec{R})$, where Γ specifies the paths traced by a set of one or more electron and hole loops.^{22,23} By Stokes' theorem $W_\Gamma = \exp(i\Phi_\Gamma)$, where $\Phi_\Gamma = \int_\epsilon d\vec{S} \cdot \vec{B}$ is the magnetic flux through the one or more loops specified by Γ , and ϵ is the sum of the surfaces bounded by those loops. This is the fundamental reason why magnetic fields have units of inverse area.

We formalize these ideas using the loop representation of observables.²⁴ The previous discussion can be summarized by the statement that every physical observable $\mathcal{O}_i(\vec{B})$ must be written as

$$\mathcal{O}_i(\vec{B}) = \sum_{\Gamma} \langle \mathcal{O}_i | \Gamma \rangle \exp(i\Phi_\Gamma) \quad (1)$$

where \sum_{Γ} is a sum over all the Wilson loops which contribute to the observable \mathcal{O}_i , and $\langle \mathcal{O}_i | \Gamma \rangle$ is the weight with which a particular Wilson loop Γ contributes to \mathcal{O}_i . This weight is determined by both the observable and by the kinetics and interactions of the electrons tracing the loops in Γ .

We specialize to the case of a uniform magnetic field \vec{B} originating externally to the sample, which allows us to assign to each Wilson loop a vector-valued cross-section $\vec{A}_\Gamma = \int_\epsilon d\vec{S}$, a vector generalization of the Wilson loop's surface area. The magnetic flux through Γ is then $\Phi_\Gamma = \vec{A}_\Gamma \cdot \vec{B}$, leading to our central result:

$$\mathcal{O}_i(\vec{B}) = \int d\vec{A} \mathcal{O}_i(\vec{A}) \exp(i\vec{A} \cdot \vec{B}), \quad (2)$$

$$\mathcal{O}_i(\vec{A}) \equiv \sum_{\Gamma} \langle \mathcal{O}_i | \Gamma \rangle \delta(\vec{A}_\Gamma - \vec{A})$$

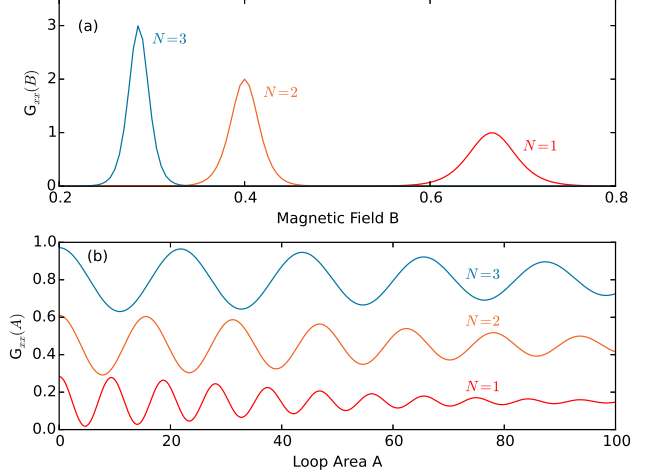


FIG. 1: (Color online.) The hierarchy of Landau levels. Panel (a) shows the magnetoconductance $G_{xx}(B)$ of the the $N = 1, 2, 3$ levels and panel (b) shows their loop area distributions $G_{xx}(A)$, which have been vertically shifted for clarity.²⁵ The repetition of levels at multiples $(N + \frac{1}{2})A_F$ of the characteristic area $A_F = E_F^{-1}$ is caused by quantum coherence. Decoherence caused by either the scattering energy scale Γ or temperature T causes wider peaks in $G_{xx}(B)$, suppression of $G_{xx}(A)$ at large A , and complete suppression of oscillations when the field B is as small as Γ, T . $E_F = 1$, $\Gamma = 0$, $T = 0.05$.

In other words, every physical observable can be resolved into contributions corresponding to specific areas \vec{A} , each with weight $\mathcal{O}_i(\vec{A})$:

$$\mathcal{O}_i(\vec{A}) = \int \frac{d\vec{B}}{(2\pi)^3} \mathcal{O}_i(\vec{B}) \exp(-i\vec{A} \cdot \vec{B}) \quad (3)$$

In summary, magnetotransport (or indeed any other observable that is sensitive to magnetic field) is directly linked to a geometrical description of the area traced out by electron loops. In particular, the external field \vec{B} is conjugate to a specific area \vec{A} , $A_i = B_i^{-1}$, and there is no possibility that any process could renormalize this relation. The loop area distribution $\mathcal{O}_i(\vec{A})$, which completely describes how different loops contribute, can be determined by simply measuring $\mathcal{O}_i(\vec{B})$ and then performing the Fourier transform from magnetic field \vec{B} to area \vec{A} .⁶⁸

To illustrate this, consider the case where the dominant energy scale is the Fermi level E_F , in which case a delta function - the first Landau level - will be found in $G_{xx}(B)$ at $B^{-1} = \frac{1}{2}A_F$. Here $2\pi/A_F \propto 2\pi E_F$ is the cross-section of the Fermi surface.²⁶ The loop area distribution is therefore a cosine $G_{xx}(A) \propto \cos(A/\frac{1}{2}A_F)$, shown in Figure 1b, which means that loops with every area contribute to the conductance and that there is ringing corresponding to the characteristic Fermi area A_F .⁶⁹

The most interesting result here is that quantum coher-

ence causes the first Landau level to be repeated exactly at characteristic areas $(N+1/2)A_F$, with the N -th level's height proportional to N . The repetitions are manifested as hierarchies of additional delta functions in $G_{xx}(B)$, as illustrated in Figure 1a. Figure 1b shows the loop area distribution $G_{xx}(A)$, where the repetitions manifest as lower frequency oscillations $\cos(A/(N + \frac{1}{2})A_F)$. In other words, quantum coherence ensures that if an electron can complete a loop once, then it can repeat that same loop any number of times. The N -th Landau level corresponds to repeating a loop $N + 1$ times.

The only limit to these repetitions is decoherence caused by the scattering energy scale Γ or temperature T , which causes a power law decay in the loop area distribution.²⁵ Decoherence broadens the Landau levels into peaks with width Γ, T , which eventually merge into SdH oscillations. These oscillations have equal height instead of the height proportional to N seen in Landau levels. They decay exponentially when the value of $B = N^{-1}A_F^{-1}$ descends to Γ, T , and their loop area distribution decays exponentially at areas larger than Γ^{-1}, T^{-1} .²⁵

We now apply the geometric interpretation to 2-D weak antilocalization, which is caused by Wilson loops Γ composed of pairs of electron and hole loops, called Cooperons, which have charge $q_C = 2e$. These pairs are much more robust against disorder than single electrons, whose phase is randomized after each scattering. In contrast, the phases of a Cooperon's electron and hole cancel each other because the two follow the same sequence of scattering events in reversed order. The WAL contribution to the conductance $G_{xx}^{WAL}(B)$ is determined by assuming that disorder causes Cooperons to move diffusively (random walks) and that their area is limited by an infrared cutoff $A_{max} = L_{max}^2$. At magnetic fields larger than the inverse cutoff $q_C B > 1/L_{max}^2$ the conductance is a logarithm $G_{xx}^{WAL}(B) \propto -\ln B$, and at smaller fields it quickly transitions to zero. The transition is quadratic in B because time reversal symmetry requires that G_{xx} be even under $B \rightarrow -B$. Aside from minor numerical changes, this log-quadratic combination is universal for both Dirac and $p^2/2m$ dispersions, for both lattice and continuum models, for both short and long range scattering, and for a wide variety of quasi-2-D geometries.²⁷⁻⁴⁰

We demonstrate here that $G_{xx}(B) \propto \ln B$ implies that the loop area distribution varies inversely with area, i.e. $G_{xx}(A) \propto A^{-1}$. The main difficulty is controlling the ultraviolet and infrared cutoffs, so we perform the demonstration three ways. First, we use purely dimensional analysis: $G_{xx}(A) = (2\pi)^{-1} \int dB \exp(-iAB) \ln B$ and therefore must carry units of inverse area. Second, we use specific functional forms for $G_{xx}(A)$ and carry out the Fourier transform analytically. For instance, if we use hard cutoffs at A_0 and A_{max} then we arrive at $G_{xx}^{WAL}(B) \approx R_0 - \ln |q_C B| + (q_C B A_0)^2/4$ for $1/A_{max} < q_C B < 1/A_0$, where $R_0 = -\gamma_E - \ln |A_0|$ and γ_E is the Euler-Mascheroni constant. Here R_0 should be adjusted to zero, as a regularization compensating for

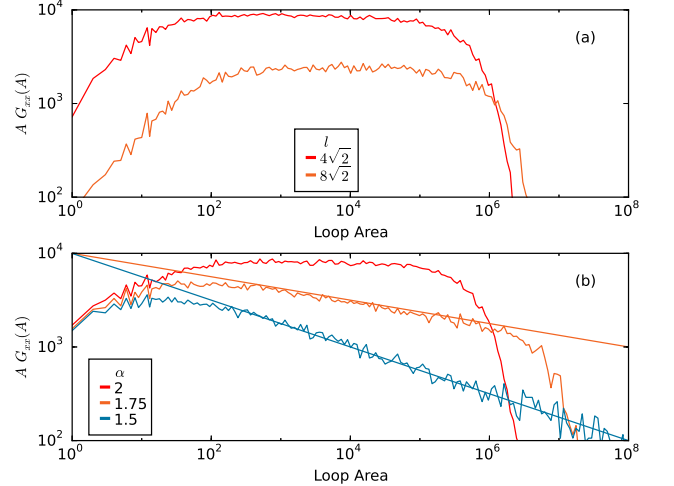


FIG. 2: (Color online.) The Cooperon's loop area distribution $G_{xx}(A)$ obtained by Monte Carlo simulations. Panel (a) shows $G_{xx}(A)$, multiplied by A , of standard 2-D random walks with Gaussian-distributed steps having average length $l = 4\sqrt{2}, 8\sqrt{2}$. The plateaus extending over several orders of magnitude verify that 2-D random walks follow an A^{-1} loop area distribution. The IR cutoff is caused by limiting the walk length to 5×10^5 . Panel (b) shows that Levy flights have a loop area distribution which decays faster than A^{-1} . α is the stability parameter of the Levy alpha-stable distribution which controls the step lengths. $\alpha = 2$ produces Gaussian-distributed steps, and when α is decreased below 2 the distribution develops a heavy tail of very long steps. The straight lines are for $10^4 \times A^{-0.125}$ and $10^4 \times A^{-0.25}$, and their agreement with the Monte Carlo data shows that $G_{xx}(A) \propto A^{-2+\alpha/2}$. $l = 4\sqrt{2}$ and the IR cutoff is 5×10^5 , 1.5×10^6 , and 5×10^6 for the $\alpha = 2, 1.75, 1.5$ results.

the hard cutoffs, in order to make the conductance be always positive. Analytical results can be obtained for other cutoffs, and invariably produce logarithmic forms for $G_{xx}(A)$. Lastly, Figure 2a summarizes the results of extensive numerical Monte Carlo simulations of random walks, all of which verify that $G_{xx}(A) \propto A^{-1}$.

This result can be reversed and applied to the case of linear magnetoresistance, where $G_{xx}(B) \propto B^{-1}$. The loop area distribution is therefore logarithmic, $G_{xx}(A) \propto -\ln A$. This profile, whose broad features are general for any roughly linear resistance, is remarkably different from the A^{-1} distribution that governs loops generated by random walks. It has fewer small loops and many more large loops; a small head and a very long tail. We emphasize that the logarithmic loop area distribution is a rigorous result and can be inferred whenever a linear magnetoresistance is seen, no matter what physical mechanism is responsible for producing the loops.

Both the logarithmic area distribution $-\ln A$ associated with linear magnetoresistance and the standard WAL result $1/A$ are monotonically decreasing functions of A , without any hint of oscillations. This contrasts very

strongly with the area profiles of Landau levels and SdH oscillations. It is very compelling evidence that linear magnetoresistance is caused by Cooperons, i.e. paired particles and holes, rather than by any species of single-particle motion. The phase of single electrons and holes oscillates very rapidly at the Fermi wavelength, which is ultimate reason why the loop area distribution of Landau levels exhibits an oscillating sign. In contrast the Cooperon phase varies at the much longer localization length, resulting in a very smooth single-sign loop area distribution.

It is difficult to explain the logarithmic area distribution's long tail using completely random walks. Increasing the dimensionality produces a steeper decay, $A^{-3/2}$ in 3-D.⁴¹ If instead diffusion is replaced by Levy flights where step lengths follow a distribution including both short and very long steps, the result is again a steeper decay than A^{-1} , because long steps tend to decrease the probability that the walker's path will complete a loop. Figure 2b shows that $G_{xx}(A) \propto A^{-2+\alpha/2}$, where $\alpha \leq 2$ is the Levy distribution stability parameter which controls the step lengths.

We propose instead that the Cooperons responsible for linear magnetoresistance do follow random walks, but with the special feature that they maintain quantum coherence, allowing them to repeat their loops many times, in the same way that Landau levels are repeated in a hierarchy at $(N + \frac{1}{2})A_F$. This depletes the loop distribution's head, because if a loop area distribution has a UV cutoff at A_0 , then its $N = 2$ first repetition will have a higher UV cutoff at $2A_0$, its third repetition will have its cutoff at $3A_0$, etc. Therefore between A_0 and $2A_0$ the total loop area distribution will have a contribution from only the base $N = 1$ loop distribution, while at larger areas higher and higher N will contribute. For example, consider the case of 2-D random walks with hard cutoffs at A_0 and A_{max} and $G_{xx}^1(B, A_0, A_{max}) = \int_{A_0}^{A_{max}} dA \cos(q_C B A)/A$. Allowing up to N repetitions with inverse weighting and regularizing with γ_E obtains $G_{xx}(B) = \gamma_E + \sum_{n=1}^N n^{-1} G_{xx}^1(B, nA_0, A_{max})$. Figure 3a compares this loop area distribution to the diffusive $1/A$ profile, showing that it has the required a small head and long tail. Figure 3b shows the resulting linear magnetoresistance, which is proportional to $R_{xx}(B) - R_{xx}(B = 0) \approx \pi q_C B A_0$ for $1/A_{max} < q_C B < 0.2/A_0$. This result is remarkable both for its clear linearity and for the excellent agreement of its slope $\pi q_C A_0$ with experimental results on cuprates and pnictides, which we will discuss later.

Linear magnetoresistance does not require the IR cutoff A_{max} , i.e. the area scale where phase coherence is suppressed, to be very large. For instance, a length of 100\AA would allow linear magnetoresistance to extend down to $\approx 0.3\text{T}$. Our formula for the linear magnetoresistance does show oscillations above $q_C B > 0.2/A_0$ which are caused by the hard UV cutoff, but with a suitably chosen UV cutoff the linear growth will extend to larger B . We emphasize that a power law area distribution can always

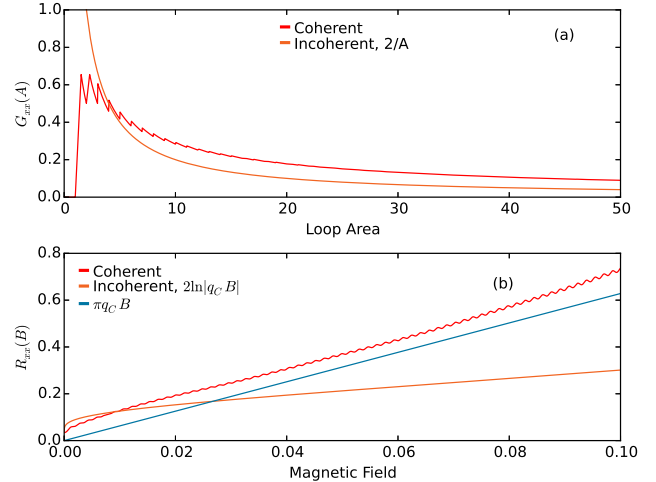


FIG. 3: (Color online.) Linear magnetoresistance from quantum coherence. $G_{xx}(A)$ is shown in panel (a) and $R_{xx}(B)$ in panel (b). Panel (a)'s red line shows the loop area distribution $G_{xx}(A)$ which is obtained by allowing loops from the $1/A$ diffusive distribution to repeat up to $N = 100$ times. This distribution clearly has a small head and long tail as compared to the standard $2/A$ incoherent distribution (orange line). Panel (b)'s red line shows the magnetoresistance obtained from quantum coherence with $N = 100$ repetitions, which compares nicely to the blue straight line with slope πq_C . The ripple is caused by the IR cutoff $A_{max} = 2000$, and $A_0 = 1$. The orange line gives a logarithmic curve from diffusion without coherence, $R_{xx}(B) = (0.1 - 2 \ln |q_C B|)^{-1}$.

be given a depleted head and long tail by invoking quantum coherence and allowing loop repetitions. The form of the UV and IR cutoffs, the relative weight of each repetition, and even the base loop area distribution $G_{xx}^1(A)$ may be specific to the scattering source and to the mechanism responsible for Cooperon coherence. Nonetheless there are only two fundamental requirements: a scattering process producing an area distribution with broad support across a range of areas, and quantum coherence allowing Cooperon loops to repeat in a hierarchy like that of Landau levels.

Ordinarily Cooperons do not maintain the coherence required to repeat their loops. Only the center of mass of the Cooperon's particle and hole is protected from scattering. The particle and hole can independently explore positions which are far from each other, and when they do so their relative position quickly loses phase coherence, which is equivalent to randomizing the Cooperon's momentum.

At least two avenues are available for guaranteeing Cooperon coherence in the presence of scattering. In certain materials transport may be locally one-dimensional, as seen in snake states in graphene, or in edge states in the quantum Hall effect, or perhaps in C_4 symmetry-broken states in underdoped cuprates.⁴²⁻⁴⁵ In other words, Cooperons may be constrained to

move along racetrack-like trajectories. Locally one-dimensional transport would imply locking between the Cooperon's position and momentum, protecting its phase coherence even when its trajectory is altered by scattering. A second route to coherence is to explicitly invoke strong correlations. For example, there has been much speculation that cuprates and pnictides above the superconducting transition host preformed pairs, precursors of superconducting Cooper pairs which at temperatures above T_c maintain phase coherence up to a length scale λ_ϕ , and which at lower temperatures unite into the superconducting condensate. The phase coherence of these preformed pairs may play a role in protecting the Cooperon's phase coherence at scales similar to λ_ϕ .

We turn to the linear-in-temperature resistance observed in bad metals. As we have seen, the loop area distribution has a smooth logarithmic form with only two characteristic area scales: the UV cutoff A_0 , and the infrared cutoff A_{max} caused by quantum decoherence. The linear magnetoresistance $R_{xx}(B) = \pi q_C B A_0$ corresponds to a logarithmic loop area distribution $G_{xx}(A) \approx -(\pi A_0)^{-1} \ln |A|$, which should be regularized to give positive values. One possible regularization is to add $(\pi A_0)^{-1} \ln |A_{max}|$. Integrating the logarithm gives $R_{xx}(B = 0) \approx \pi A_0 / A_{max}$ for $A_0 \ll A_{max}$, plus regularization-dependent terms which are sensitive to the cutoffs. When A_{max} is comparable to A_0 the inverse dependence on A_{max} collapses. At larger A_{max} the inverse dependence is robust because B^{-1} and A_{max} both act at large length scales and therefore are roughly interchangeable.

The ultraviolet cutoff A_0 may be controlled by many length scales: the spin relaxation length with its crossover from WAL to WL, the scattering length, the lattice spacing, the scale of the Fermi surfaces, etc. These mechanisms depend weakly on temperature. Turning to A_{max} , we remind that quantum coherence governs the loop area distribution, and its tail reflects events where Cooperons repeat the same loop many times. Regardless of which short distance physics such as scattering contributes to the loop area distribution of Cooperon loops (prior to coherence-based repetitions), this physics has no control over the repetitions or the infrared cutoff A_{max} . After repetition the loop area distribution has loops far larger than those caused by pure diffusion, which indicates that A_{max} is not controlled by the scattering length. The *only* thing which controls A_{max} is quantum decoherence, which is controlled by temperature. As seen in SdH oscillations, decoherence occurs when the inverse area A_{max}^{-1} matches the energy scale set by temperature T . In summary, no area scale except inverse temperature can influence $A_{max} \propto T^{-1}$, and therefore $R_{xx}(B = 0) \approx \pi A_0 / A_{max}$ must exhibit linear-in-temperature resistance.

The constant of proportionality between A_{max}^{-1} and T has been obtained experimentally by measuring the coefficient $\alpha k_B T$ of linear temperature dependence and the coefficient $\beta \mu_B B \approx \beta \mu_B A_{max}^{-1}$ of linear field depen-

dence, and then taking their ratio $\gamma = \alpha / \beta$.⁷⁰ Hayes et al measured γ in the high- T_c pnictide superconductor $\text{BaFe}_2(\text{As}_{1-x}\text{P}_x)_2$ at dopings ranging between 0.31 and 0.41, and found that γ was identical to one in atomic units, within their experimental error bar of 7%.¹⁸ Further studies of $\text{La}_{2-x}\text{Sr}_x\text{CuO}_4$ and $\text{Yb}_{1-x}\text{La}_x\text{Rh}_2\text{Si}_2$ at various dopings near optimal doping have found constants between 0.7 and 2.3.^{18,19} We conclude that γ does depend on the substrate, but only mildly, and that it is of order 1; i.e. $A_{max} \approx (2T)^{-1}$ and $R_{xx}(B = 0) \approx 2\pi T A_0$.

The value of exactly one for γ is easily explained by combining the Heisenberg uncertainty relation with a $p^2/2m$ dispersion: $B^{-1} = A = \langle (\Delta x)^2 \rangle = \hbar^2 / \langle p^2 \rangle$, where the momentum scale is determined by $\langle p^2 / 2m_e \rangle = T$. The Heisenberg relation is a quantum mechanical upper bound on the decoherence scale which can be obtained at a given temperature. These arguments indicate that $\gamma = m/m_e$ measures the effective mass of the charge carriers. The experimental observation of $\gamma = 1$, i.e. a $p^2/2m_e$ dispersion, implies that the electrons and holes which contribute to the Cooperon are unbound with bare electron mass m_e . Like a plasma, they are insensitive to the ionic potential of their substrate. This conclusion is consistent with other works on bad metals, which find that strong correlations in these materials cause the spectral density to have a very wide support on the energy axis.

Ref. 46 determined the linear coefficient η of the linear-in-temperature resistance $R_{xx}(B = 0) = \eta T$ in four cuprates: $\text{La}_{2-x}\text{Sr}_x\text{CuO}_4$ (LSCO), $\text{YBa}_2\text{Cu}_3\text{O}_{6+\delta}$ (YBCO), $\text{Tl}_2\text{Ba}_2\text{CuO}_{6+\delta}$ (Tl2201), and $\text{HgBa}_2\text{CuO}_{4+\delta}$ (Hg1201). They found that this coefficient is universal in the cuprates if one uses the sheet resistance per CuO_2 plane, not per unit cell. After conversion to atomic units, the linear coefficient is $\eta = 2\pi \times 32 a_0^2 \times p^{-1}$, where $0 \leq p \leq 1$ is the doping, i.e. the number of holes per unit cell, not per CuO_2 plane.⁷¹ We surmise on dimensional grounds that the linear coefficient η should not depend on the doping, but instead on the carrier density 2-D ρ_{2D} . Using $p = \rho_{2D} \times \mathcal{A}$ where $\mathcal{A} \approx 53a_0^2$ is the cross-section of the unit cell in the cuprates' copper oxide plane, we arrive at $R_{xx}(B = 0) = 0.60 \times 2\pi \times (\rho_{2D})^{-1} \times T$. This suggests that the UV cutoff A_0 of the loop area distribution is simply the inverse of the carrier density, i.e. $A_0 = \rho_{2D}^{-1}$, and that (at least in the cuprates) our formulas for the resistance should be multiplied by a dimensionless normalization factor $\mathcal{N} = 0.60$. This normalization factor \mathcal{N} may reflect details of the Cooperon coherence mechanism and the UV and IR cutoffs. It is remarkable that \mathcal{N} is close to one, especially because when we selected the loop area distribution prior to coherence-induced repetitions, we chose the most obvious normalization: 1 in atomic units. On this grounds our formula's $\mathcal{N} = 1$ could be called a prediction, and if so it is remarkably well fulfilled by the cuprates. The experimental $\mathcal{N} = 0.60 \approx 1$ is all the more remarkable in comparison to the normalization of the standard WAL conductance, which is $(2\pi)^{-2} \ll 1$. This may be a sign that Cooperon

coherence in the cuprates belongs to a universality class which is independent of many UV details, and suggests that the same factor may extend to the pnictides. In any case, using $A_0 = \rho_{2D}^{-1}$ and the normalization factor \mathcal{N} immediately results in $R_{xx}(B) = \mathcal{N} \times \pi q_C \rho_{2D}^{-1} B$ and $R_{xx}(T) = \mathcal{N} \times 2\pi \rho_{2D}^{-1} T$. Where the carrier mass m differs from the bare electron mass m_e , the resistance will be multiplied by m/m_e . These formulas offer the possibility of determining the charge carrier density directly from either the linear magnetoresistance or the linear in temperature resistance, without any speculation about the material's chemistry or band structure.

We turn to the bad metal's weak-field regime and the small-temperature regime, which are distinct. Time reversal symmetry, combined with the presence of a fairly sharp (faster than power law) infrared cutoff A_{max} , requires a B^2 behavior at small fields, i.e. $\rho = \rho_0 + (B/B_0)^2$. This was found in both Ref. 18 and Ref. 19. In particular, Ref. 18 verified that $\rho = \rho_0 + (\mu_B B/T)^2/2$ in $\text{BaFe}_2(\text{As}_{1-x}\text{P}_x)_2$ and found a smooth form which interpolates between small and large fields: $\rho_0 + \sqrt{B^2 + T^2}$. This form does not give a general description of the small T limit because finite B does not impose a sharp cutoff on the integral $G_{xx}(B) = \int dA \exp(iAB) G_{xx}(A)$. Therefore the small T behavior may be sensitive to the tail of the loop area distribution $G_{xx}(A)$. In point of fact Ref. 18 saw a quadratic form in $\text{BaFe}_2(\text{As}_{1-x}\text{P}_x)_2$ which indicates that in this material $G_{xx}(A)$ decays slowly compared to the experimental values of B^{-1} , while Ref. 19 saw a linear form in $\text{La}_{2-x}\text{Sr}_x\text{CuO}_4$ indicating a sharper cutoff. Systematic studies of the tail of $G_{xx}(A)$ throughout the high- T_c phase diagram are likely to be very illuminating. Such studies require only an increased attention to the magnetoconductance's sensitivity to small changes in B . Any sharp cutoff (faster than power law) at A_{max} will manifest in the magnetoconductance as fast ripples with period $2\pi A_{max}$, which will be visible even at large fields. Using $A_{max} = (2T)^{-1}$, at $T = 0.1\text{K}$ the ripple period will be 0.93 Tesla.

Since we have established that the temperature in bad metals determines a decoherence area $A_{max} = (2T)^{-1}$, the critical temperature T_c at which bad metals superconduct should be interpreted as simply a 2-D critical density $\rho_c = 2T_c$. When the decoherence area satisfies $A_{max} \times \rho_c > 1$ superconductivity occurs. The conversion from $2T_c$ to ρ_c is performed by first converting $2T_c$ to atomic units of energy (Rydbergs), and (using $m_e = \hbar = 1$) interpreting the resulting numerical value as a density in units of a_0^{-2} , where a_0 is the Bohr radius. For example, in YBCO at optimal doping $T_c = 93.5\text{K}$ and $\rho_c \approx 1/(470\text{\AA}^2)$. Values of the effective electron mass m larger than the bare mass m_e will multiply ρ_c by m/m_e .

It is natural to interpret the critical density ρ_c as one half of the density of electron or hole carriers which participate in superconductivity. This would lead to

$$\rho_c = \frac{\rho_{2D}}{2} \times \mathcal{E} \quad (4)$$

TABLE I: Analysis of the critical density at which superconductivity occurs. T_c is the superconducting critical temperature, p is the optimal doping, ρ_{2D} is the carrier sheet density, the critical density $\rho_c = A_{max}^{-1}$ is the inverse of the area $A_{max} = (2T_c)^{-1}$ which limits coherence, and the efficiency factor $\mathcal{E} = 2\rho_c/\rho_{2D}$ is the fraction of carriers which participate in superconductivity. The pnictides' superconducting domes are flat with very weak variations in T_c as the doping is varied by a factor of two or even four, and there are corresponding uncertainties in ρ_{2D} and \mathcal{E} . References: YBa₂Cu₃O_{6+δ} (YBCO)⁴⁷, Bi₂Sr_{2-z}La_zCuO_{6+δ} (BSLCO)^{48,49}, HgBa₂Ca₄Cu₅O_{12+δ} (Hg-1245)^{50,51}, Bi₂Sr₂Ca₂Cu₃O_{10+δ} (Bi2223)^{52,53}, annealed monolayer FeSe^{54,55}, SmO_{1-x}F_xFeAs (SmOFeAs)⁵⁶, LaFeAsO_{1-x}H_x (LaOFeAs)^{57,58}.

	$T_c[\text{K}]$	p	$\rho_{2D}^{-1}[\text{\AA}^2]$	$\rho_c^{-1}[\text{\AA}^2]$	\mathcal{E}
YBCO	93.5	0.161	92	470	0.39
BSLCO	38	0.16	91	1160	0.16
Hg-1245	110	0.236	63	400	0.31
Bi2223	110	0.22	134	400	0.67
Bi2223, 36 GPa	136	0.22	135	325	0.83
FeSe	65	0.12	118	680	0.35
SmOFeAs	55	0.20	80	800	0.19
LaOFeAs	36	0.30	54	1230	0.09
LaOFeAs, 6 GPa	52	0.18	90	850	0.21

where ρ_{2D} is the carrier sheet density and \mathcal{E} is an efficiency factor, i.e. the fraction of carriers which participate in superconductivity. We take ρ_{2D} to be the sheet density per unit cell, which results in lower values of the efficiency than those obtained by using instead the sheet density per CuO₂ plane. Table I reports the values of ρ_{2D} , ρ_c , and the \mathcal{E} for several cuprates and pnictides. It is encouraging that all of the efficiencies satisfy the upper bound $\mathcal{E} \leq 1$, i.e. the number of carriers inside A_{max} is not smaller than two, and that the efficiencies are generally within an order of magnitude of this bound. On the other hand, it is noteworthy that in most cases the efficiency \mathcal{E} is significantly lower than 1, indicating that many of the carriers do not assist in the superconducting transition. One possible reason is that in some materials the effective mass of the carriers may exceed m_e , in which case $\rho_c = 2T_c \times m/m_e$ and therefore $\mathcal{E} = 2\rho_c/\rho_{2D}$ should be corrected by a factor of m/m_e compared to the values reported here. Another possibility is that some of the carriers may be pinned in place by local variations in the sample, and the onset of superconductivity may be a percolative transition, as unpinned carriers meet and establish phase coherence. Indeed, the logarithmic form of the bad metal loop area distribution indicates that some Cooperon loops are quite small, and these loops would be less likely to participate in percolation and macroscopic coherence than larger loops. On the other hand Bi2223 attains an efficiency $\mathcal{E} = 0.83$, implying that there is no fundamental barrier to attaining at least this efficiency. Sample defects may also be responsible for reducing the number of carriers; if so then T_c will decrease linearly

with the number of sample defects, as seen in Ref. 59.

We turn to the underdoped sector of the cuprate phase diagram. Our formula $T_c \propto \rho_{2D} \propto p$ predicts that T_c is proportional to p and goes to zero at zero doping $p = 0$. This contrasts with Presland's well-known quadratic formula for the superconducting dome, which exceeds the linear prediction by as much as 17% in the interval $0.09 < p < 0.16$ and outside of that interval drops rapidly, reaching $T_c = 0$ at $p = 0.05$.⁶⁰ The quadratic formula however neglects the 1/8 anomaly which depresses T_c near $p = 0.125$. The fact that $T_c = 0$ occurs at $p = 0.05$ is probably connected with cuprates' antiferromagnetic phase transition at small doping. The transition could depress T_c either by causing the carriers' effective mass to diverge or by depleting the number of carriers.⁶¹

In the underdoped cuprate phase diagram there is a second energy scale, the pseudogap temperature T_{pg} , which is characterized by a transition from linear-in-temperature resistance above T_{pg} to another dependence at smaller temperatures.⁴⁸ Presumably T_{pg} is also evident in the magnetoconductance. Like T_c , the pseudogap temperature is linear in the doping, but unlike T_c its slope has a much larger magnitude and is negative. Near zero doping T_{pg} is close to the Neel temperature, and near the overdoped side of the superconducting dome it reaches $T_{pg} = 0$. Using the data of Ref. 48 we find that the pseudogap's slope in Kelvin per hole doping is -2100K for BSLCO, -1500K for LSCO, and -2200K for YBCO. Using the same logic as for T_c , we define a density $\rho_{pg} = 2T_{pg}$ and a pseudogap efficiency $\mathcal{E}_{pg} = -2\rho_{pg}/\rho_{2D}$, and we find that the efficiency is 1.4 for BLSO, 1.0 for LSO, and 1.5 for YBCO. Considering the uncertainty associated with extraction of T_{pg} from the raw transport data, these numbers indicate that the pseudogap efficiency is equal to the identity. In other words, if we define a density of pseudogap carriers ρ_{pg} equal to a constant ρ_{Total} minus the density of holes i.e. $\rho_{pg} + \rho_{2D} = \rho_{Total}$, then at the pseudogap transition temperature T_{pg} the number of pseudogap carriers inside the decoherence area A_{max} is equal to two. The constant ρ_{Total} is approximately equal to the number of holes at the overdoped side of the superconducting dome, and may be determined by the Neel temperature. In summary, it seems that changing the hole doping converts pseudogap carriers to superconducting carriers, and that the total number of carriers is constant.

Overall, our analysis suggests three routes for increasing T_c . A first direction is to decrease the carrier mass m , since $\rho_c = 2T_c \times \frac{m}{m_e}$ is proportional to the carrier mass. Unfortunately the data of Refs. 18,19 suggest that in $\text{BaFe}_2(\text{As}_{1-x}\text{P}_x)_2$, $\text{La}_{2-x}\text{Sr}_x\text{CuO}_4$, and $\text{Yb}_{1-x}\text{La}_x\text{Rh}_2\text{Si}_2$ near optimal doping the carrier mass is quite close to the bare electron mass, suggesting that in these materials further improvement will be difficult unless the carrier mass can be reduced below m_e . A second direction is to increase the efficiency factor \mathcal{E} , i.e. the percentage of carriers which participate in supercon-

ductivity, for instance by removing defects which might pin carriers in place. Here the use of thicker unit cells may be helpful, since 3-D transport tends to be more resilient against localization than 2-D transport. Most of the materials in Table I would have T_c 's between 200K and 300K, which is near the cuprates' Neel temperature, if they reached full efficiency $\mathcal{E} = 1$. The third direction is to find a way to increase the carrier density ρ_{2D} while retaining phase coherence and delaying the transition into a Fermi liquid state. This would likely require a deeper understanding both of scattering and of the mechanism responsible for phase coherence, including any locally one dimensional physics at small scales. In the cuprates it might involve increasing the Neel temperature. Going beyond the cuprates, it is encouraging that the pnictides' superconducting domes are flat and extend to dopings and carrier densities far larger than those of the cuprates, which hints that we may still be far from saturating any fundamental upper bound on the doping or carrier density.

If, as we have suggested, WAL is responsible for the bad metals' linear resistance, then a diffuse (non-momentum-conserving) component should be seen in the density of states and in excitation spectra. This is in fact true in the cuprates and pnictides. In principle the scattering could be caused by anything that fluctuates at a time scale longer than the time required to go around a loop. If the scattering source is truly static, then Universal Conductance Fluctuations should be seen in the magnetoconductance, and possibly individual phase coherent loops will be visible to STM experiments. UCFs have not been reported in bad metals, although very few studies of the magnetoconductance have been performed. If UCFs cannot be found in bad metals above T_c , this would indicate that scattering is caused by fluctuations within the material. In this case one would see time dependent fluctuations and possibly glassy behavior, as found in Refs. 62,63 using transport measurements and in Ref. 64 using muon spin relaxation.

Lastly we point out that, in our view, one of the most important aspects of the present work is its methodology, which focuses on geometric analysis of electron and hole loops, and especially on the loop area distribution that can be obtained from Fourier transforms of magnetoconductance data. We have presented a non-perturbative framework for understanding fermion behavior that is completely independent of any assumptions about Fermi liquid physics and gives additional physical insight. We anticipate experiments focusing on the loop area distribution, with special attention to accessing large areas using carefully controlled small increments of the field, to removing leads effects, and to performing careful Fourier transforms. We also expect increased use of vector magnets and multi-dimensional Fourier transforms.

Acknowledgments

We gratefully acknowledge formative and stimulating discussions with S. Kettemann, Y. Li, C. Lin, X. Dai, V. Dobrosavljevic, H.-J. Lee, Q. Wu, T. Ohtsuki, J. Zaanen,

T. Takimoto, K.-S. Kim, X. Wan, P. Niklowitz, and S. Hayden. We also thank A. Leggett for correspondence, and especially A. Petrovic who discussed the manuscript during preparation. We acknowledge support from EPSRC grant EP/M011038/1.

* Electronic address: vincent@sacksteder.com

- ¹ S. X. Zhang, R. D. McDonald, A. Shekhter, Z. X. Bi, Y. Li, Q. X. Jia, and S. T. Picraux, *Applied Physics Letters* **101**, 202403 (2012).
- ² W. Zhang, R. Yu, W. Feng, Y. Yao, H. Weng, X. Dai, and Z. Fang, *Phys. Rev. Lett.* **106**, 156808 (2011).
- ³ X. Wang, Y. Du, S. Dou, and C. Zhang, *Phys. Rev. Lett.* **108**, 266806 (2012).
- ⁴ J. Feng, Y. Pang, D. Wu, Z. Wang, H. Weng, J. Li, X. Dai, Z. Fang, Y. Shi, and L. Lu, *Phys. Rev. B* **92**, 081306 (2015).
- ⁵ F. Kisslinger, C. Ott, C. Heide, E. Kampert, B. Butz, E. Specker, S. Shallcross, and H. B. Weber, *Nature Physics* **11**, 650 (2015).
- ⁶ C. Zhang, C. Guo, H. Lu, X. Zhang, Z. Yuan, Z. Lin, J. Wang, and S. Jia, *Phys. Rev. B* **92**, 041203 (2015).
- ⁷ K. Wang, D. Graf, and C. Petrovic, *Phys. Rev. B* **89**, 125202 (2014).
- ⁸ X. Xu, W. H. Jiao, N. Zhou, Y. Guo, Y. K. Li, J. Dai, Z. Q. Lin, Y. J. Liu, Z. Zhu, X. Lu, et al., *Journal of Physics: Condensed Matter* **27**, 335701 (2015).
- ⁹ Y. Sun, S. Pyon, and T. Tamegai, *Phys. Rev. B* **93**, 104502 (2016).
- ¹⁰ Y. Tanabe, K. K. Huynh, S. Heguri, G. Mu, T. Urata, J. Xu, R. Nouchi, N. Mitoma, and K. Tanigaki, *Phys. Rev. B* **84**, 100508 (2011).
- ¹¹ D. Bhoi, P. Mandal, P. Choudhury, S. Pandya, and V. Ganesan, *Applied Physics Letters* **98**, 172105 (2011).
- ¹² J. Fenton and A. J. Schofield, *Phys. Rev. Lett.* **95**, 247201 (2005).
- ¹³ A. E. Koshelev, *Phys. Rev. B* **88**, 060412 (2013).
- ¹⁴ A. A. Abrikosov, *Phys. Rev. B* **58**, 2788 (1998).
- ¹⁵ T. Khouri, U. Zeitler, C. Reichl, W. Wegscheider, N. E. Hussey, S. Wiedmann, and J. C. Maan, *Phys. Rev. Lett.* **117**, 256601 (2016).
- ¹⁶ M. M. Parish and P. B. Littlewood, *Nature* **426**, 162 (2003).
- ¹⁷ N. E. Hussey, K. Takenaka, and H. Takagi, *Philosophical Magazine* **84**, 2847 (2004).
- ¹⁸ I. M. Hayes, R. D. McDonald, N. P. Breznay, T. Helm, P. J. Moll, M. Wartenbe, A. Shekhter, and J. G. Analytis, *Nature Physics* **12**, 916 (2016).
- ¹⁹ P. Giraldo-Gallo, J. A. Galvis, Z. Stegen, K. A. Modic, F. F. Balakirev, J. B. Betts, X. Lian, C. Moir, S. C. Riggs, J. Wu, et al., arXiv preprint arXiv:1705.05806 (2017).
- ²⁰ X. Deng, J. Mravlje, R. Žitko, M. Ferrero, G. Kotliar, and A. Georges, *Phys. Rev. Lett.* **110**, 086401 (2013).
- ²¹ S. A. Hartnoll, *Nature Physics* **11**, 54 (2015).
- ²² K. G. Wilson, *Phys. Rev. D* **10**, 2445 (1974).
- ²³ R. P. Feynman, *Phys. Rev.* **80**, 440 (1950).
- ²⁴ A. Ashtekar and C. Rovelli, *Classical and Quantum Gravity* **9**, 1121 (1992).
- ²⁵ B. Laikhtman and E. L. Altshuler, *Annals of Physics* **232**, 332 (1994).
- ²⁶ L. Onsager, *The London, Edinburgh, and Dublin Philosophical Magazine and Journal of Science* **43**, 1006 (1952).
- ²⁷ S. Hikami, A. I. Larkin, and Y. Nagaoka, *Progress of Theoretical Physics* **63**, 707 (1980).
- ²⁸ B. L. Altshuler and A. G. Aronov, *JETP Lett.* **33**, 499 (1981).
- ²⁹ V. K. Dugaev and D. E. Khmelnitskii, *Sov. Phys. JETP* **59**, 1038 (1984).
- ³⁰ G. Bergmann, *Phys. Rev. B* **39**, 11280 (1989).
- ³¹ O. E. Raichev and P. Vasilopoulos, *Journal of Physics: Condensed Matter* **12**, 589 (2000).
- ³² J. S. Meyer, A. Altland, and B. L. Altshuler, *Phys. Rev. Lett.* **89**, 206601 (2002).
- ³³ I. Garate and L. Glazman, *Phys. Rev. B* **86**, 035422 (2012).
- ³⁴ C. W. J. Beenakker and H. van Houten, *Phys. Rev. B* **38**, 3232 (1988).
- ³⁵ C. J. Lin, X. Y. He, J. Liao, X. X. Wang, V. S. IV, W. M. Yang, T. Guan, Q. M. Zhang, L. Gu, G. Y. Zhang, et al., *Phys. Rev. B* **88**, 041307 (2013).
- ³⁶ V. E. Sacksteder, K. B. Arnardottir, S. Kettemann, and I. A. Shelykh, *Phys. Rev. B* **90**, 235148 (2014).
- ³⁷ Q. Wu and V. E. Sacksteder, *Phys. Rev. B* **90**, 045408 (2014).
- ³⁸ K. Nomura, M. Koshino, and S. Ryu, *Phys. Rev. Lett.* **99**, 146806 (2007).
- ³⁹ J. H. Bardarson, J. Tworzydło, P. W. Brouwer, and C. W. J. Beenakker, *Phys. Rev. Lett.* **99**, 106801 (2007).
- ⁴⁰ C. H. Lewenkopf, E. R. Mucciolo, and A. H. Castro Neto, *Phys. Rev. B* **77**, 081410 (2008).
- ⁴¹ D. V. Baxter, R. Richter, M. L. Trudeau, R. W. Cochrane, and J. O. Strom-Olsen, *Journal de Physique* **50**, 1673 (1989).
- ⁴² L. Oroszlány, P. Rakyta, A. Kormányos, C. J. Lambert, and J. Cserti, *Phys. Rev. B* **77**, 081403 (2008).
- ⁴³ T. K. Ghosh, A. De Martino, W. Häusler, L. Dell'Anna, and R. Egger, *Phys. Rev. B* **77**, 081404 (2008).
- ⁴⁴ J. R. Williams and C. M. Marcus, *Phys. Rev. Lett.* **107**, 046602 (2011).
- ⁴⁵ K. Fujita, C. K. Kim, I. Lee, J. Lee, M. H. Hamidian, I. A. Firmino, S. Mukhopadhyay, H. Eisaki, S. Uchida, M. J. Lawler, et al., *Science* **344**, 612 (2014).
- ⁴⁶ N. Barišić, M. K. Chan, Y. Li, G. Yu, X. Zhao, M. Dressel, A. Smontara, and M. Greven, *Proceedings of the National Academy of Sciences* **110**, 12235 (2013).
- ⁴⁷ G. Grissonnanche, O. Cyr-Choinière, F. Laliberté, S. R. De Cotret, A. Juneau-Fecteau, S. Dufour-Beauséjour, M.-E. Delage, D. LeBoeuf, J. Chang, B. J. Ramshaw, et al., *Nature Communications* **5**, 3280 (2014).
- ⁴⁸ Y. Ando, S. Komiya, K. Segawa, S. Ono, and Y. Kurita, *Phys. Rev. Lett.* **93**, 267001 (2004).
- ⁴⁹ M. D. Biegalski, E. Crumlin, A. Belianinov, E. Muto, Y. Shao-Horn, and S. V. Kalinin, *Applied Physics Letters* **104**, 161910 (2014).
- ⁵⁰ H. Mukuda, Y. Yamaguchi, S. Shimizu, Y. Kitaoka, P. Shiraishi, and A. Iyo, *Journal of the Physical Society of Japan*

⁵¹ J. Z. Wu, *Physica C: Superconductivity* **493**, 96 (2013).

⁵² H. P. Roeser, F. Hetfleisch, F. M. Huber, M. F. von Schoenemann, M. Stepper, A. Moritz, and A. S. Nikoghosyan, *Acta Astronautica* **63**, 1372 (2008).

⁵³ X.-J. Chen, V. V. Struzhkin, Y. Yu, A. F. Goncharov, C.-T. Lin, H.-K. Mao, and R. J. Hemley, *Nature* **466**, 950 (2010).

⁵⁴ S. He, J. He, W. Zhang, L. Zhao, D. Liu, X. Liu, D. Mou, Y.-B. Ou, Q.-Y. Wang, Z. Li, et al., arXiv preprint arXiv:1207.6823 (2012).

⁵⁵ F.-C. Hsu, J.-Y. Luo, K.-W. Yeh, T.-K. Chen, T.-W. Huang, P. M. Wu, Y.-C. Lee, Y.-L. Huang, Y.-Y. Chu, D.-C. Yan, et al., *Proceedings of the National Academy of Sciences* **105**, 14262 (2008).

⁵⁶ R. Zhi-An, L. Wei, Y. Jie, Y. Wei, S. Xiao-Li, Zheng-Cai, C. Guang-Can, D. Xiao-Li, S. Li-Ling, Z. Fang, et al., *Chinese Physics Letters* **25**, 2215 (2008).

⁵⁷ S. Iimura, S. Matsuishi, H. Sato, T. Hanna, Y. Muraba, S. W. Kim, J. E. Kim, M. Takata, and H. Hosono, *Nature Communications* **3**, 943 (2012).

⁵⁸ H. Takahashi, H. Soeda, M. Nukii, C. Kawashima, T. Nakanishi, S. Iimura, Y. Muraba, S. Matsuishi, and H. Hosono, *Scientific reports* **5**, 7829 (2015).

⁵⁹ F. Rullier-Albenque, H. Alloul, and R. Tourbot, *Phys. Rev. Lett.* **91**, 047001 (2003).

⁶⁰ M. R. Presland, J. L. Tallon, R. G. Buckley, R. S. Liu, and N. E. Flower, *Physica C: Superconductivity* **176**, 95 (1991).

⁶¹ S. E. Sebastian, N. Harrison, M. M. Altarawneh, C. H. Mielke, R. Liang, D. A. Bonn, D. N. Hardy, and G. G. Lonzarich, *Proceedings of the National Academy of Sciences* **107**, 6175 (2010).

⁶² I. Raičević, J. Jaroszyński, D. Popović, C. Panagopoulos, and T. Sasagawa, *Phys. Rev. Lett.* **101**, 177004 (2008).

⁶³ G. R. Jelbert, T. Sasagawa, J. D. Fletcher, T. Park, J. D. Thompson, and C. Panagopoulos, *Phys. Rev. B* **78**, 132513 (2008).

⁶⁴ C. Panagopoulos, A. P. Petrovic, A. D. Hillier, J. L. Tallon, C. A. Scott, and B. D. Rainford, *Phys. Rev. B* **69**, 144510 (2004).

⁶⁵ G. P. Mikitik and Y. V. Sharlai, *Phys. Rev. Lett.* **82**, 2147 (1999).

⁶⁶ N. Nagaosa and P. A. Lee, *Phys. Rev. Lett.* **64**, 2450 (1990).

⁶⁷ A. J. Leggett, *Quantum liquids: Bose condensation and Cooper pairing in condensed-matter systems* (Oxford University Press, 2006).

⁶⁸ In the systems of interest here the spin relaxation length is short and therefore the spin triplet component of the single particle density does not contribute to transport. When this is not the case it will be useful to extend the geometric analysis advocated here to a special relativistic formulation where electron/hole loops extend both in time and position (4 dimensions), loop areas $A^{\mu\nu}$ have six components (three rotations and three boosts), the conjugate to area is the electromagnetic tensor $F^{\mu\nu}$ which contains both \vec{B} and \vec{E} , and the physical observables are $\mathcal{O}_i(F^{\mu\nu})$ and $\mathcal{O}_i(A_{\mu\nu})$. This extension allows seamless treatment of the spin degree of freedom, and its (2 + 1) dimensional version is natural for analysis of Hall bar experiments.

⁶⁹ A slightly different result $\cos(A/NA^F)$ obtains for the N -th Landau level of Dirac fermions.⁶⁵

⁷⁰ In this discussion of the proportionality between A_{max}^{-1} and T we neglect the Cooperon charge q_C , which does not affect γ .

⁷¹ Up to the multiplicative constant, this formula $R \propto T/p$ is the same as Ref. 66's RVB result. See also Ref. 67 for discussion of the resistance per CuO₂ plane.